Modification of electronic structure induced by local lattice distortion in Li_3GaN_2 and Li_3AlN_2: Simulation by a discrete variational $X\alpha$ method

K. Kushida*
Department of Arts and Sciences, Osaka Kyoiku University, Kashiwara, Osaka 582-8582, Japan

K. Kuriyama
College of Engineering and Research Center of Ion Beam Technology, Hosei University, Tokyo 184-8584, Japan
(Received 21 June 2007; revised manuscript received 24 August 2007; published 26 December 2007)

The relationship between the bonding character and local lattice distortion in cubic Li_3GaN_2 (Li_3AlN_2), which is structurally analogous to zinc blende GaN (AlN) whose empty tetrahedral sites are filled with Li, is studied by the discrete variational (DV) $X\alpha$ method. The DV-$X\alpha$ simulation clarifies that the Li-N bonds in Li_3GaN_2 (Li_3AlN_2) are almost ionic, whereas the Ga-N (Al-N) bonds consist of a mixture of covalent and ionic characters. The simulation also shows that with increasing local lattice distortion arising from the difference in length between the Li-N and Ga-N (Al-N) bonds, the ionicity of the Ga-N (Al-N) bond increases, whereas the covalency of the Ga-N (Al-N) bond and the ionicity of the Li-N bond remain almost constant. The simulated dependencies of the energy gaps (E_g's) of Li_3GaN_2 and Li_3AlN_2 on local lattice distortion are also reported, showing that the calculated E_g of Li_3GaN_2 approaches that of Li_3AlN_2. This similarity of the calculated E_g correlates with the increase in the contribution of the Li $2p$ orbital components to the conduction band bottoms of both compounds. The difference in calculated E_g (ΔE_g=0.4 eV) between the Li_3GaN_2 and Li_3AlN_2 cluster models with actual local lattice distortions (9.3% for Li_3GaN_2 and 12.6% for Li_3AlN_2) is consistent with the difference in experimental E_g (ΔE_g=0.25 eV), suggesting that the small difference in experimental E_g reflects the similarity of the ionicity of the Li-N bonds.

DOI: 10.1103/PhysRevB.76.245124 PACS number(s): 71.20.Nr, 71.90.+q, 71.15.Ap

I. INTRODUCTION

Wurtzite AlN and GaN are wide energy gap semiconductors with potential applications in high-power or optoelectronic devices. Recently, zinc-blende (ZB) AlN (Ref. 1) and GaN (Ref. 2) have been grown, and their energy gaps (E_g's) have been determined to be 5.34 eV (Ref. 1) (indirect) and 3.30 eV (Ref. 2) (direct), respectively. However, ZB GaN and AlN are metastable, whereas Nowotony-Juza nitride compounds[3–5] such as LiZnN,[6] LiMgN,[7] Li_3AlN_2,[8] and Li_3GaN_2 (Ref. 9) have cubic phases and may be considered as alternatives to ZB GaN or ZB AlN. LiZnN can be viewed as a ZB GaN-like [$(ZnN)^-$] lattice whose empty tetrahedral sites next to N atoms are filled with He-like Li^+ ions.[10] Based on the "interstitial insertion rule,"[10–12] the insertion of Li^+ into empty tetrahedral sites next to N in the $(ZnN)^-$ lattice causes an upward shift in the X point of the conduction band because of the Pauli repulsion between conduction electrons, which exposes Γ as the conduction band minimum and converts indirect band gap materials into direct ones. Although the band gap of LiZnN has been confirmed to be direct ($E_g \sim 1.91$ eV),[6] E_g of LiZnN was much smaller than that of GaN. Therefore, we aimed at Li_3AlN_2 (Ref. 8) and Li_3GaN_2 (Ref. 9), another type of filled tetrahedral semiconductor with many ionic Li-N bonds, to study wide-energy-gap materials.

In previous studies, we synthesized Li_3AlN_2 (a =9.427 Å) (Ref. 8) and Li_3GaN_2 (a=9.605 Å) (Ref. 9) polycrystalline samples which were confirmed to be the single phases of Li_3AlN_2 and Li_3GaN_2, respectively. The E_g values of actual Li_3AlN_2 (4.40 eV) (Ref. 8) and Li_3GaN_2 (4.15 eV) (Ref. 9) were also experimentally determined by optical absorption and photoacoustic spectroscopy methods. We also demonstrated that E_g of Li_3AlN_2 is direct,[8] which was followed by a first principles calculation.[13] The experimental E_g of Li_3AlN_2 (4.40 eV) is close to that of Li_3GaN_2 (4.15 eV), which leads to our interpretations[9] that each E_g is essentially determined by Li-N ionic bonds, and that the difference in covalency between Ga-N and Al-N bonds results in a slight difference in E_g between Li_3AlN_2 and Li_3GaN_2. However, as reported by Juza and co-workers,[3,5] note that the Al-N (Ga-N) bond is 12.6% (9.3%) shorter than the Li-N bond in actual Li_3AlN_2 (Li_3GaN_2), leading to the local lattice distortion of 12.6% (9.3%), as described later. Although our experiments cause another question how the local distortion affects the electronic structure of Li_3AlN_2 (Li_3GaN_2), we have encountered technological difficulties to synthesize Li_3AlN_2 (Li_3GaN_2) samples with various local lattice distortions. Accordingly, detailed considerations based on a first principles calculation are necessary to verify the correlation between their electronic structures and local lattice distortions in both compounds.

In this study, using the discrete vibrational (DV) $X\alpha$ method, we calculate the bonding character and E_g of the Li_3AlN_2 (Li_3GaN_2) cluster models with various local lattice distortion to clarify how its electronic structure correlates with local lattice distortion. Note that the local lattice distortions in the Li_3AlN_2 (Li_3GaN_2) cluster models are determined by the calculation on the basis of the assumption that the Li-N bond [the Al-N (Ga-N) bond] in the cluster models expand [shrink] in the same direction as in actual Li_3AlN_2 (Li_3GaN_2). The ionicity of the Ga-N (Al-N) bond increases with local lattice distortion, whereas the covalency of the Ga-N (Al-N) bond and the ionicity of the Li-N bond remain

almost constant. The calculated E_g of Li_3GaN_2 approaches that of Li_3AlN_2 with increasing local lattice distortion. Additionally, we compare the difference in calculated E_g between both compounds possessing actual local lattice distortions (9.3% for Li_3GaN_2 and 12.6% for Li_3AlN_2) with the difference in experimental E_g.

II. CRYSTAL STRUCTURES OF Li_3GaN_2 AND Li_3AlN_2

Figure 1(a) shows a unit cell of Li_3GaN_2 (Li_3AlN_2), which is depicted without local lattice distortion for clarity. In the unit cell, N atoms occupy 8*a* [e.g., (0, 0, 0)] and 24*d* [e.g., (1/4, 1/4, 0)] sites, and Ga (Al) and Li atoms occupy 16*c* [e.g., (1/8, 1/8, 1/8)] and 48*e* [e.g., (1/8, 3/8, 1/8)] sites, respectively,[3,5] where 8*a*, 24*d*, 16*c*, and 48*e* are the Wyckoff symbols. The N atoms at 8*a* and 24*d* sites are referred to as $N_{(a)}$ and $N_{(d)}$, respectively. The unit cell consists of a cubic main frame constructed by $N_{(a)}$. Both $N_{(a)}$ and $N_{(d)}$ are eightfold coordinated by two Ga (Al) and six Li nearest neighbors, as shown in Fig. 1(b). The arrows shown in Figs. 1(b) and 1(c) indicate the directions in which Li, Ga (Al), and $N_{(d)}$ atoms are displaced in actual crystals,[3,5] as will be discussed later. Ga (Al) atoms around $N_{(d)}$ are located on only one side of $N_{(d)}$, whereas those around $N_{(a)}$ are located at the diagonal sites of $N_{(a)}$ [Fig. 1(b)]. Around $N_{(d)}$, it is considered that 50% of Ga (Al) atoms in ZB GaN (AlN) are replaced by Li and its empty tetrahedral sites next to N are filled with Li. Therefore, a 1/8 sublattice in Li_3GaN_2 (Li_3AlN_2) can be viewed as a ZB GaN-like $[Li_{0.5}Ga_{0.5}N]^-$ (ZB AlN-like $[Li_{0.5}Al_{0.5}N]^-$) lattice whose empty tetrahedral sites are filled with Li^+, as shown in Fig. 1(c).

According to Juza and co-workers,[3,5] $N_{(d)}$, Ga (Al), and Li in actual Li_3GaN_2 (Li_3AlN_2) are displaced in such a manner that the Ga-N (Al-N) bond becomes 9.3% (12.6%) shorter than the Li-N bond, as indicated by the arrows in Figs. 1(b) and 1(c). For example, Ga (Al) is displaced to $(1/8-\Delta c, 1/8-\Delta c, 1/8-\Delta c)$, Li to $(1/8+\Delta x, 3/8+\Delta y, 1/8-\Delta z)$, and $N_{(d)}$ to $(1/4, 1/4-\Delta d, 0)$. The difference in length between the Ga-N (Al-N) and Li-N bonds results in lattice distortion. However, since $N_{(a)}$ atoms remain stationary even in actual Li_3GaN_2 (Li_3AlN_2), the unit cell preserves the cubic frame. Additionally, the lengths of the Li-$N_{(a)}$ and Ga-$N_{(a)}$ (Li-$N_{(a)}$ and Al-$N_{(a)}$) bonds are the same as those of the Li-$N_{(d)}$ and Ga-$N_{(d)}$ (Li-$N_{(d)}$ and Al-$N_{(d)}$) bonds, respectively. Consequently, actual Li_3GaN_2 (Li_3AlN_2) crystallizes in a cubic structure with distorted tetrahedral coordination, leading to another type of filled tetrahedral semiconductors.

III. COMPUTATION OF ELECTRONIC STRUCTURE BY DV-$X\alpha$ METHOD

Molecular orbital calculations by the DV-$X\alpha$ method are based on the technique used for calculating the electronic structures of solid-state materials by Ellis and Painter.[14] The DV-$X\alpha$ method is a linear-combination-of-atomic-orbital method within the framework of the Hartree-Fock-Slater self-consistent one-electron local density theory. The one-electron Schrödinger equation with a nonrelativistic approximation for the molecular orbital calculation is written by

$$H\Psi = E\Psi, \tag{1}$$

$$H = -\frac{P^2}{2m} + V_{eff}(r), \tag{2}$$

where Ψ is the wave function (or molecular orbitals), E the electronic energy, H the Hartree-Fock-Slater Hamiltonian

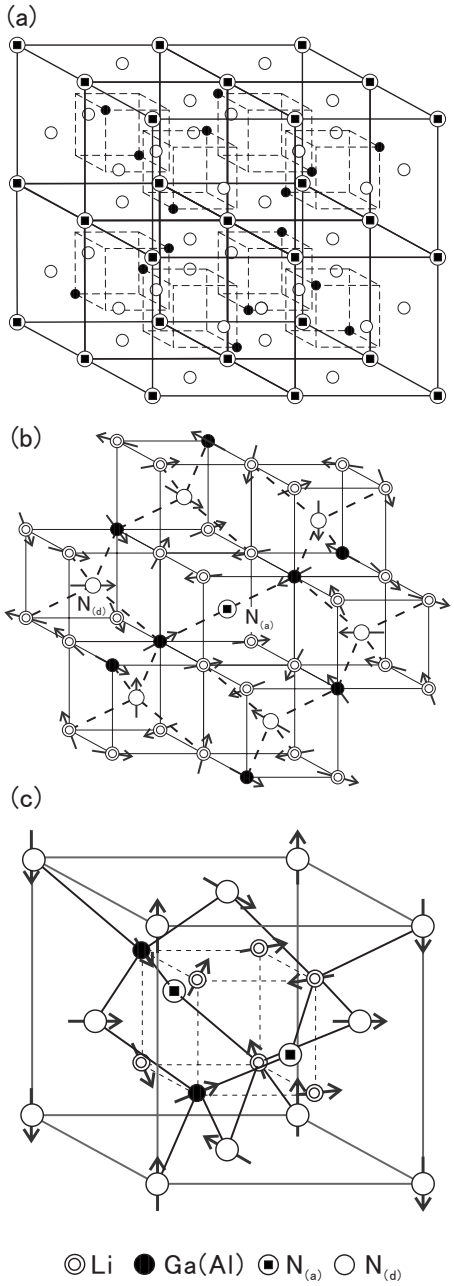

FIG. 1. (a) Unit cell of Li_3GaN_2 (Li_3AlN_2) without local distortion (space group: *Ia*3). For clarity, no Li atoms are shown here. (b) Magnification of unit cell depicted around $N_{(a)}$. Li, Ga(Al), and $N_{(d)}$ atoms are displaced from their ideal positions in the direction indicated by the arrows, whereas $N_{(a)}$ atoms remain stationary. (c) A 1/8 sublattice of Li_3GaN_2 (Li_3AlN_2).

operator, and $-P^2/2m$ the electronic kinetic energy (P the momentum operator). $V_{eff}(r)$ is the effective potential energy expressed as a function of the electronic position r,

$$V_{eff}(r) = \sum \frac{-Z_N}{|r-R_N|} + \int \frac{\rho(r')}{|r-r'|}dr' + V_{ex}(r), \qquad (3)$$

where Z_N is the atomic number, $|r\text{-}R_N|$ the distance between an electron and a nucleus, and ρ the electronic density. The first term is the Coulomb potentials from the nuclei and the second term is that from the other electrons. For the exchange potential $V_{ex}(r)$, we here used the $X\alpha$ potential proposed by Slater,[15] which is expressed as follows:

$$V_{ex}(r) = -3\alpha\left\{\frac{3}{8\pi}\rho(r)\right\}^{1/3}, \qquad (4)$$

where α is a parameter determined by setting the total energy obtained by the $X\alpha$ method. The total energy obtained by the $X\alpha$ method is equal to that obtained by the Hartree-Fock method. When using $\alpha=0.7$, errors in molecular orbital calculations are generally negligible.[16] By the DV-$X\alpha$ method, the discrete energy eigenvalues (the electronic structure) of a model cluster are self-consistently calculated using numerical atomic basis functions. The original DV-$X\alpha$ computation program was developed by Ellis and Painter,[14] and it was improved later by Rosen *et al.*,[17] Adachi *et al.*,[18] and many researchers.[19] In this study, for the nonrelativistic DV-$X\alpha$ calculation, a computation code DVSCAT (Refs. 18 and 23) was used. The DV-$X\alpha$ method has been used to interpret the optical transition in $YAl_3(BO_3)_4:Gd^{3+}$ (Ref. 20) or to predict the electronic structures of spinel $LiMn_2O_4$ (Ref. 21) and $LiInO_2$ (Ref. 22).

The cluster models for the present DV-$X\alpha$ calculations are the unit cells of Li_3GaN_2 and Li_3AlN_2 with local lattice distortion. The lattice parameters of the cluster models are the same as those of actual unit cells (9.605 Å for Li_3GaN_2 and 9.427 Å for Li_3AlN_2). The minimal basis sets used were $1s$-$2p$ for $N_{(a)}$, $1s$-$2p$ for $N_{(d)}$, $1s$-$2p$ for Li, and $1s$-$4p$ ($1s$-$3d$) for Ga (Al). The local lattice distortion in Li_3GaN_2 (Li_3AlN_2) can be represented by $(1\text{-}R_{M-N}/R_{Li-N})\times 100$ (%) [M=Ga (Al) and N=$N_{(a)}$ or $N_{(d)}$], where R is the bond length. For example, in actual Li_3AlN_2 (Li_3GaN_2), its local lattice distortion is 12.6% (9.3%), since the Al-N (Ga-N) bond is 12.6% (9.3%) shorter than the Li-N bond. To calculate the local lattice distortions, other than the distortion of 12.6% (9.3%), in the Li_3AlN_2 (Li_3GaN_2) cluster models used for the present DV-$X\alpha$ simulations, we assumed that the Li, Ga (Al), and $N_{(d)}$ atoms in the cluster models are continuously displaced in the same directions as in actual Li_3GaN_2 (Li_3AlN_2). The displacement of the Li, Ga (Al), and $N_{(d)}$ atoms in the cluster models accompanies the difference in bond length between the Li-N and the Ga-N (Al-N) bonds, leading to the local distortion calculated by $(1\text{-}R_{M-N}/R_{Li-N})\times 100$ (%) [M=Ga (Al) and N=$N_{(a)}$ or $N_{(d)}$]. The local lattice distortions in the cluster models used for the present DV-$X\alpha$ calculation are 0%, 1.0%, 2.1%, 4.4%, 6.9%, 9.3%, 12.6%, and 15.8%. The relationship between the Li-N and Ga-N (Al-N) bond lengths and the corresponding local lattice distortion in Li_3GaN_2 (Li_3AlN_2) is shown in Fig. 2. The dashed and solid lines in Fig. 2 show the same local distortions as in actual crystals (9.3% in Li_3GaN_2 and 12.6% in Li_3AlN_2). To simulate a comparable bulk crystalline state, the cluster models were under the conditions in a Madelung potential field instead of under periodical boundary conditions, as performed in previous works[20–22] by the DV-$X\alpha$ method. The approximation that used a Madelung potential field was applied to the calculation of the electronic structures of the Li_3AlN_2 and Li_3GaN_2 cluster models.

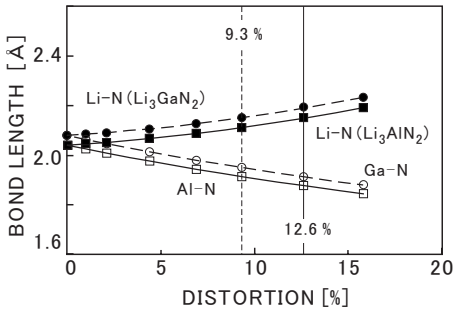

FIG. 2. Relationship between the Li-N and Ga-N (Al-N) bond lengths and the local lattice distortion in Li_3GaN_2 (Li_3AlN_2). The local distortion in Li_3GaN_2 (Li_3AlN_2) can be represented by $(1-R_{M\text{-}N}/R_{Li-N})\times 100$ (%) (M=Ga or Al and N=$N_{(a)}$ or $N_{(d)}$), where R is the bond length. The dashed and solid lines indicate the distortions of actual Li_3GaN_2 and Li_3AlN_2 crystals, respectively. These lines are also used in Figs. 3–5 and 10.

BONDING CHARACTERS OF Li_3GaN_2 AND Li_3AlN_2

The bonding characters of Li_3GaN_2 and Li_3AlN_2 are calculated through the Mulliken population analysis of their

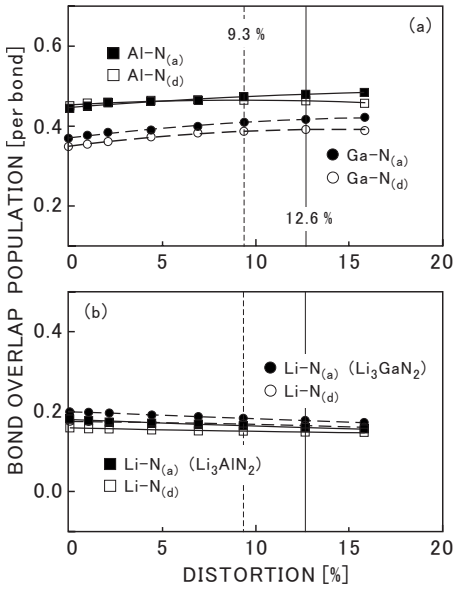

FIG. 3. Bond overlap populations (BOPs) of (a) Li-$N_{(a)}$ and Li-$N_{(d)}$ and (b) Ga(Al)-$N_{(a)}$ and Ga(Al)-$N_{(d)}$ in Li_3GaN_2 (Li_3AlN_2) vs local distortion.

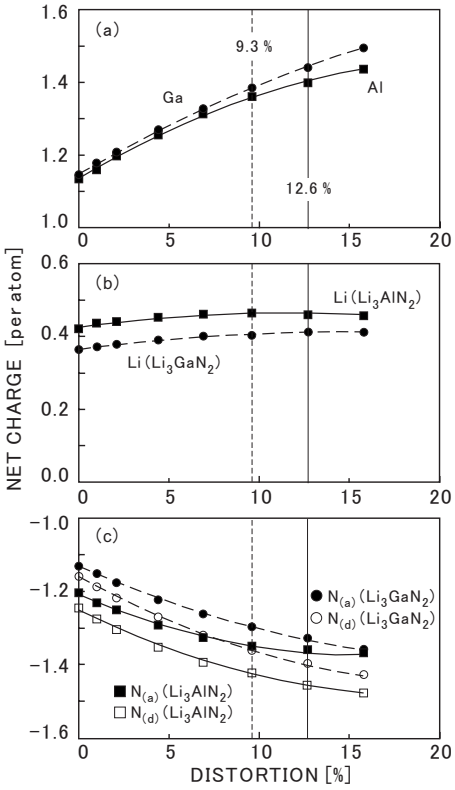

FIG. 4. Net charges (NCs) of (a) Ga(Al), (b) Li, and (c) $N_{(a)}$ and $N_{(d)}$ in Li_3GaN_2 (Li_3AlN_2) vs local distortion. Positive and negative NCs correspond to the positively and negatively ionized states, respectively.

molecular orbitals obtained from the present DV-$X\alpha$ calculation. The two complementary programs[23] BNDODR and NETC were used for the Muliken population analysis in this study. The bond overlap population (BOP) between nearest-neighbor atoms in Li_3GaN_2 (Li_3AlN_2) is considered a measure of covalency. The BOPs in Li_3GaN_2 (Li_3AlN_2) were computed by the program BNDODR.[23] The amount of transferred charges between atoms in Li_3GaN_2 (Li_3AlN_2) is also calculated, which is referred to as the net charge (NC) of Li, Ga (Al), $N_{(a)}$, or $N_{(d)}$. The NCs in Li_3GaN_2 (Li_3AlN_2) were computed by the program NETC.[23] The positive and negative NCs indicate the positively and negatively ionized states resulting from the charge transfers, respectively. Because the Li-N bond lengths of both compounds increase with local lattice distortion in contrast to the Ga-N and Al-N bond lengths, an evaluation of the Coulomb potential between M and N (M=Li, Ga, or Al and N=$N_{(a)}$ or $N_{(d)}$) is necessary to measure ionicity. Coulomb potential is expressed as $NC_{(M)} \times NC_{(N)} e^2/4\pi\varepsilon R_{M-N}$, where e is the charge of the electron and ε the dielectric constant. However, the dielectric constants of both compounds are unknown. Therefore, we used $NC_{(M)} \times NC_{(N)}/R_{M-N}$ as a measure of ionicity.

Figure 3 shows the dependencies of the BOPs of Li_3GaN_2 and Li_3AlN_2 on local lattice distortion. The BOPs of the Al-$N_{(a)}$ and Al-$N_{(d)}$ bonds are greater than those of the Ga-$N_{(a)}$ and Ga-$N_{(d)}$ bonds, and these BOPs remain almost constant over the entire local distortion range. Thus, the Al-N bonds possess a larger covalency than the Ga-N bonds, and the covalencies of both bonds are also almost constant over the entire local distortion range. On the other hand, the Li-$N_{(a)}$ and Li-$N_{(d)}$ bonds in both compounds have very small BOPs compared with the Ga-N and Al-N bonds. Moreover, the BOPs of the Li-N bonds are almost constant. Therefore, the Li-N bonds have a small covalency compared with the Ga-N and Al-N bonds, despite the fact that on the basis of our previous study (Ref. 9), we expected the Li-N bonds in both compounds to be purely ionic. The covalencies of the Li-N bonds in both compounds are also almost constant over the entire range.

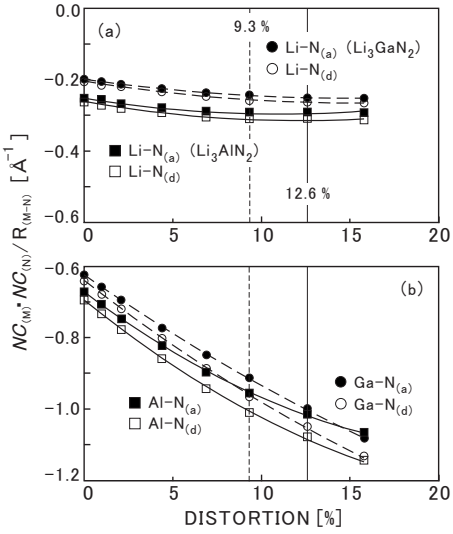

FIG. 5. $NC_{(M)} \times NC_{(N)}/R_{M-N}$ (M=Li, Ga, or Al and N=$N_{(a)}$ or $N_{(d)}$) of (a) Li-$N_{(a)}$ and Li-$N_{(d)}$ and (b) Ga(Al)-$N_{(a)}$ and Ga(Al)-$N_{(d)}$ vs local distortions, where NC is the net charge. Negative $NC_{(M)} \times NC_{(N)}/R_{M-N}$ values indicate attractive interactions between Li and N [Ga (Al) and N].

Figure 4 shows the dependencies of the NCs of Ga (Al), Li, and N in Li_3GaN_2 (Li_3AlN_2) on local distortion. It is suggested that Li and Ga (Al) give their charges to $N_{(a)}$ and $N_{(d)}$ in Li_3GaN_2 (Li_3AlN_2). Their NCs deviate from the formal charges (+3 for Ga and Al, +1 for Li, and −3 for $N_{(a)}$ and $N_{(d)}$), indicating that Ga, Al, Li, and N atoms are not purely ionized and each bond includes both ionicity and covalency. As shown in Fig. 4(a), the NC of Ga becomes larger than that of Al with increasing local distortion. In contrast, the NCs of Li in Li_3GaN_2 and Li_3AlN_2 are almost constant over the entire local distortion range, and Li in Li_3AlN_2 possesses a larger NC than that in Li_3GaN_2, as shown in Fig. 4(b). As shown in Fig. 4(c), the negative NCs of $N_{(a)}$ and $N_{(d)}$ in both compounds remarkably increase with local distortion, which coincides with the increase in the NCs of Ga and Al. The NCs of $N_{(a)}$ and $N_{(d)}$ in Li_3AlN_2 are larger than those in Li_3GaN_2, respectively, resulting from the larger amount of charge transferred from Li to N atoms in Li_3AlN_2 than in Li_3GaN_2. This is consistent with the result described in Fig. 4(b).

Figure 5 shows the dependencies of $NC_{(M)} \times NC_{(N)}/R_{M-N}$ (M=Li, Ga, or Al and N=$N_{(a)}$ or $N_{(d)}$) on

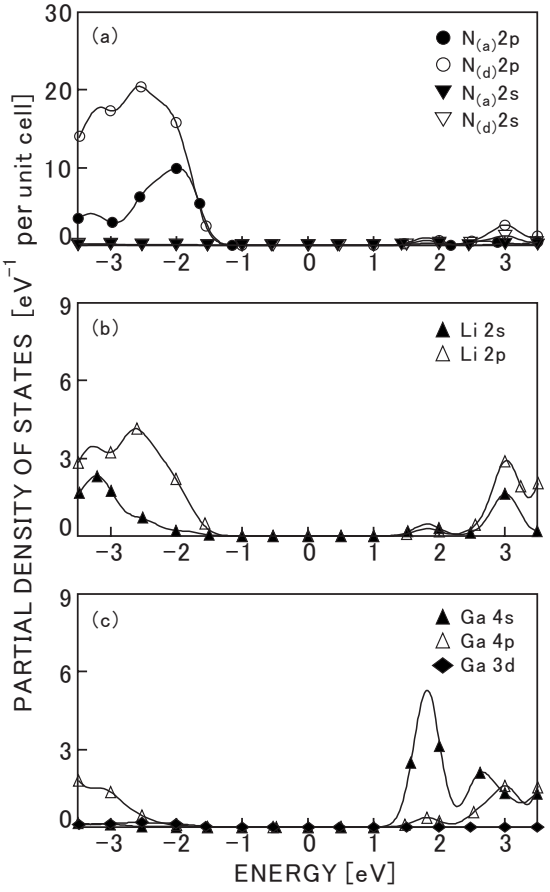

FIG. 6. Partial density of states (PDOS) diagram of Li_3GaN_2 without local lattice distortion. (a), (b), and (c) show the orbital components of N, Li, and Ga, respectively. These components are also used in Figs. 7–9.

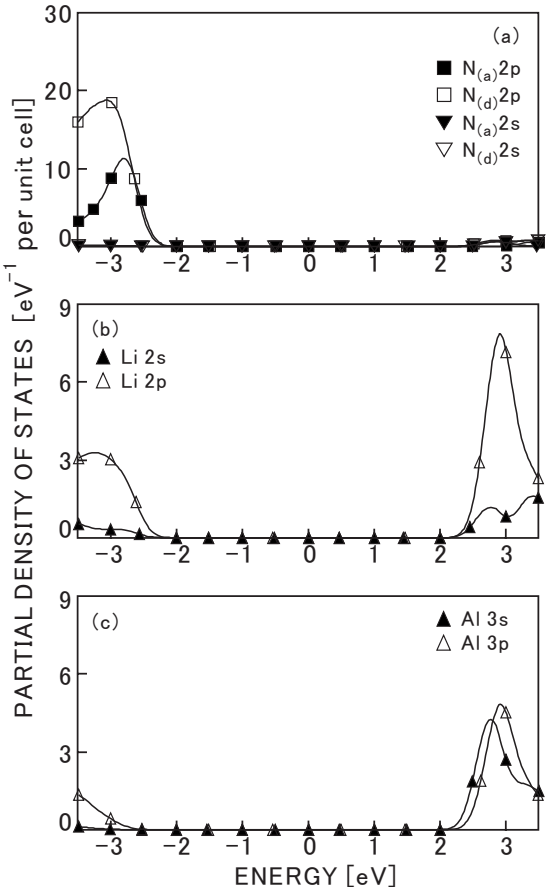

FIG. 7. PDOS diagram of Li_3AlN_2 without local lattice distortion.

local distortion. Negative $NC_{(M)} \times NC_{(N)}/R_{M-N}$ values indicate attractive interactions between Li and N [Ga (Al) and N]. As shown in Fig. 5(a), the $NC_{(Li)} \times NC_{(N)}/R_{Li-N}$ values of both compounds are almost constant through the entire local distortion range, although the negative NCs of N atoms increase with local distortion, as shown in Fig. 4(c). This is mainly attributed to the gradual increase in the Li-N bond length with local distortion. In contrast, $NC_{(Ga)} \times NC_{(N)}/R_{Ga-N}$ ($NC_{(Al)} \times NC_{(N)}/R_{Al-N}$) monotonously increases with local distortion, arising both from the increases in the NCs of Ga (Al), $N_{(a)}$, and $N_{(d)}$, as shown in Fig. 4, and from the decrease in Ga-N (Al-N) bond length, as shown in Fig. 2. Thus, the ionicities of the Ga-N and Al-N bonds increase with local distortion over the entire local distortion range, whereas those of the Li-N bonds in both compounds are almost constant. Furthermore, the $NC_{(M)} \times NC_{(N)}/R_{Ga(Al)-N}$ of Ga-$N_{(d)}$ (Al-$N_{(d)}$) bond shows a larger increase than that of the Ga-$N_{(a)}$ (Al-$N_{(a)}$) bond, suggesting that the ionicity of the Ga-$N_{(d)}$ (Al-$N_{(d)}$) bond is greater than that of the Ga-$N_{(a)}$ (Al-$N_{(a)}$) bond. This reflects the difference in the location of Ga (Al) around N between $N_{(a)}$ and $N_{(d)}$, which arises from the fact that Ga (Al) atoms around $N_{(d)}$ are located on only one side of $N_{(d)}$ and those around $N_{(a)}$ are located at diagonal sites of $N_{(a)}$ [see Fig. 1(b)].

V. ENERGY GAPS OF Li_3GaN_2 AND Li_3AlN_2

The E_g values of Li_3GaN_2 and Li_3AlN_2 are determined from the difference between the highest occupied molecular orbital (HOMO) and lowest unoccupied molecular orbital (LUMO) levels in this study, although the HOMO-LUMO gap estimated by the DV-$X\alpha$ method generally leads to the overestimation of E_g.

To clarify orbital components that contribute to the conduction and valence band edges, the partial density of states (PDOS) is calculated for Li, Ga (Al), and N atoms. Figures 6 and 7 show the PDOS diagrams of Li_3GaN_2 and Li_3AlN_2 without local lattice distortion, respectively. The PDOS diagrams for 9.3% distorted Li_3GaN_2 and 12.6% distorted Li_3AlN_2 are also shown in Figs. 8 and 9, respectively. All the PDOS diagrams (Figs. 6–9) were depicted by artificially broadening the discrete energy eigenvalues using Gaussian functions, as preformed in previous works[20–22] by the DV-$X\alpha$ method. The full width at half maximum (FWHM) smaller than 0.5 eV of the Gaussian function has been generally used for this purpose.[20–22] Therefore, the FWHM of 0.2 eV is chosen in this study to fit the calculated band gap,

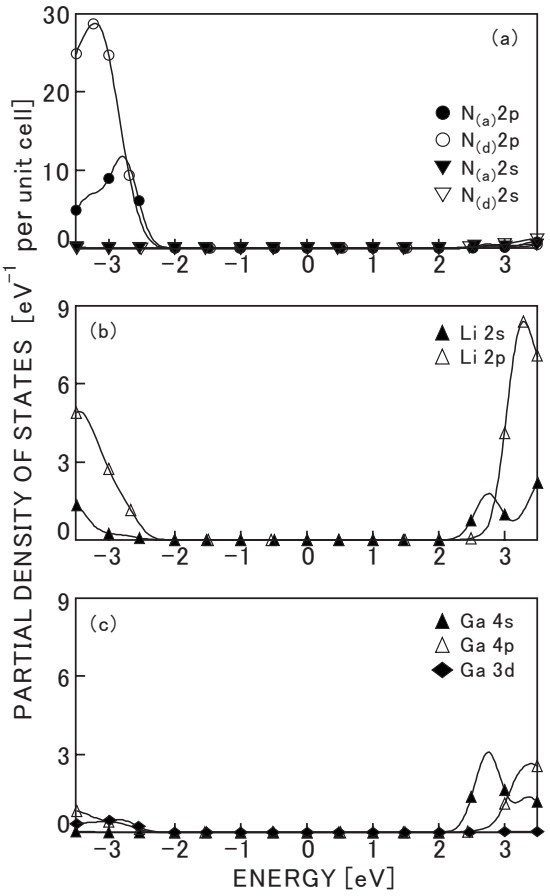

FIG. 8. PDOS diagram of Li_3GaN_2 with 9.3% distortion.

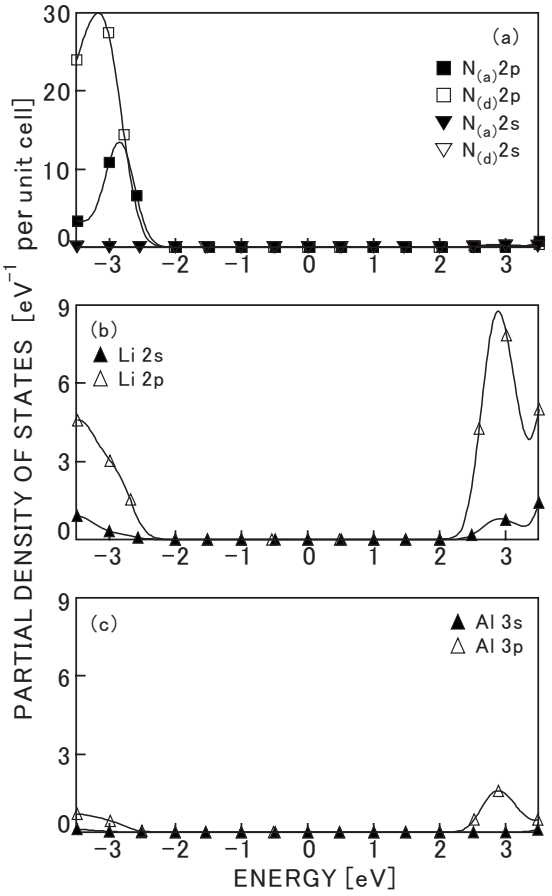

FIG. 9. PDOS diagram of Li_3AlN_2 with 12.6% distortion.

which are determined from the total DOS of the 12.6% distorted Li_3AlN_2 (the 9.3% distorted Li_3GaN_2) cluster model to the experimental E_g of actual Li_3AlN_2 (Li_3GaN_2). On the top of the valence bands of both compounds, $N_{(d)}$ $2p$ and $N_{(a)}$ $2p$ orbitals are predominant in both cases without and with local distortion, as shown in Figs. 6–9. In the case without distortion in Li_3GaN_2, the bottom of the conduction band is mainly composed of the Ga $4s$ orbital component, as shown in Fig. 6. On the other hand, in Li_3AlN_2, the Li $2p$ component predominates at the bottom of the conduction band, although the contributions of the Al $3s$ and Al $3p$ components are comparable to that of the Li $2p$ component, as shown in Fig. 7.

At local distortions up to 9.3% in Li_3GaN_2, the Ga $4s$ orbital component predominates at the bottom of the conduction band, as shown in Fig. 8; however, the contribution of the Li $2s$ component gradually increases and becomes comparable to that of the Ga $4s$ component. At a local distortion of 12.6%, the contribution of the Li $2s$ component exceeds that of the Ga $4s$ component. Finally, at a distortion of 15.8%, the contribution of the Li $2p$ orbital component becomes predominant. On the other hand, in Li_3AlN_2, the contribution of the Li $2p$ component is predominant over the entire local distortion range. Up to a distortion of 6.9%, the contributions of the Al $3s$ and Al $3p$ orbital components rapidly decrease. At distortions above 9.3%, the contribution of the Li $2p$ component becomes entirely predominant, as shown in Fig. 9.

Figure 10 shows the calculated dependencies of the E_g values of Li_3GaN_2 and Li_3AlN_2 on local distortion. In the case without local lattice distortion, Li_3AlN_2 has an E_g value 1.9 eV larger than that of Li_3GaN_2, as shown in Fig. 10, which is analogous to the E_g difference between ZB GaN (Ref. 2) (3.3 eV) and AlN (Ref. 2) (5.34 eV). The E_g difference between Li_3GaN_2 and Li_3AlN_2 is mainly attributed to the larger covalency of Al-N bonds in Li_3AlN_2 than that of Ga-N bonds in Li_3GaN_2, since the bottom of the conduction bands in Li_3AlN_2 and Li_3GaN_2 consists of large contributions of the Ga and Al orbital components, respectively. With increasing local distortion, E_g of Li_3GaN_2 increases and reaches its maximum at a distortion of 9.3%, whereas E_g of Li_3AlN_2 only slightly increases up to a local distortion of 6.9%. The increase in E_g of Li_3GaN_2 coincides with the considerable increase in the ionicity of Ga-N bonds. Therefore, E_g of Li_3GaN_2 is strongly affected by the increase in the ionicity of Ga-N. E_g of Li_3AlN_2 is weakly affected by the increase in the ionicity of Al-N bonds, because the contribution of the Al orbital components is small due to its rapid decrease. E_g of Li_3GaN_2 (Li_3AlN_2) gradually decreases when the distortion in Li_3GaN_2 (Li_3AlN_2) reaches 12.6% (9.3%). Furthermore, the E_g values of Li_3GaN_2 and Li_3AlN_2 approach each other at distortions above 12.6% and 9.3%, respectively, indicating a correlation between the variation in E_g and the increase in the contribution of the Li $2p$ component. Thus, at distortions above 12.6% (9.3%), E_g of

Li_3GaN_2 (Li_3AlN_2) is mainly affected by the ionicity of Li-N bonds. In particular, the difference in the calculated E_g between the 9.3% distorted Li_3GaN_2 and the 12.6% distorted Li_3AlN_2 cluster models is 0.4 eV, which is consistent with the difference in experimental E_g (ΔE_g=0.25 eV) (Refs. 8 and 9) between actual Li_3GaN_2 and Li_3AlN_2. In the 9.3% distorted Li_3GaN_2 cluster, the contribution of the Ga 4*s* orbital component is still large near the bottom of the conduction band, as discussed in this study, and however, the contribution of the Li 2*s* component is comparable to that of the Ga 4*s* component in actual Li_3GaN_2. In the 12.6% distorted Li_3AlN_2 cluster, the contribution of the Li 2*p* orbital component is predominant. Therefore, the difference in covalency between the Ga-N and Al-N bonds does not result in the difference in E_g. In our previous study,[9] we described that the small difference in the experimental E_g between both compounds is attributed to the difference in covalency between the Ga-N and Al-N bonds. However, these simulation results indicate that the small difference in the experimental E_g between actual Li_3GaN_2 and Li_3AlN_2 is mainly attributed to the similarity of the ionicity of the Li-N bonds.

VI. CONCLUSION

The relationship between the local lattice distortion and bonding character of cubic Li_3GaN_2 (Li_3AlN_2) is studied by the DV $X\alpha$ method. The Li-N bonds in Li_3GaN_2 and Li_3AlN_2 are almost ionic, while the Ga-N (Al-N) bond consists of a mixture of both covalent and ionic characters. With increasing local distortion, the ionicity of the Ga-N (Al-N) bond increases, whereas the covalency of the Ga-N (Al-N) bond and the ionicity of the Li-N bond remain almost constant. In the case without the distortion, Li_3AlN_2 possesses an energy gap which is 1.9 eV larger than that of Li_3GaN_2, mainly reflecting the higher covalency of the Al-N bonds than the Ga-N bonds. With increasing local lattice distortion, the calculated E_g of Li_3GaN_2 approaches that of Li_3AlN_2, mainly reflecting the similar ionicities of the Li-N bonds in both compounds. The difference in calculated E_g [ΔE_g =0.4 eV] between the Li_3GaN_2 and Li_3AlN_2 cluster models with actual local lattice distortions (9.3% for Li_3GaN_2 and 12.6% for Li_3AlN_2) is consistent with the difference in experimental E_g [ΔE_g=0.25 eV (Refs. 8 and 9)].

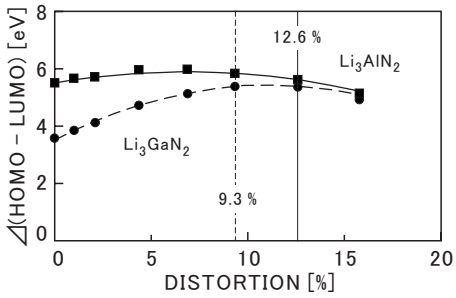

FIG. 10. Calculated energy gaps between highest occupied molecular orbital (HOMO) and lowest unoccupied molecular orbital (LUMO) levels of Li_3GaN_2 and Li_3AlN_2 vs local distortion.

Further experiments such as optical band gap, x-ray absorption fine structure, and Raman scattering measurements of single Li_3AlN_2 and Li_3GaN_2 crystals under high pressure are required to prove the results of the present simulation.

ACKNOWLEDGMENTS

The present work was supported in part by a Grant-in-Aid for Young Scientists (B) from the Japanese Ministry of Education, Culture, Sports, Science and Technology (No.18760013), and was also partly supported by the Kansai Research Foundation for Technology Promotion and the CASIO Science Promotion Foundation. The authors would like to thank Hisashi Yoshida of Kansei Gakuin University for helpful advice on the DV-$X\alpha$ molecular orbital method.

*Corresponding author; kkushi@cc.osaka-kyoiku.ac.jp

[1] M. P. Thompson, G. W. Auner, T. S. Zheleva, K. A. Jones, S. J. Simko, and J. N. Hilfiker, J. Appl. Phys. **89**, 3331 (2001).
[2] J. Menniger, U. Jahn, O. Brandt, H. Yang, and K. Ploog, Phys. Rev. B **53**, 1881 (1996).
[3] R. Juza and F. Hund, Z. Anorg. Chem. **257**, 1 (1948).
[4] R. Juza and F. Hund, Z. Anorg. Chem. **257**, 13 (1948).
[5] R. Juza, K. Langer, and K. V. Benda, Angew. Chem., Int. Ed. Engl. **7**, 360 (1968).
[6] K. Kuriyama, T. Kato, and T. Tanaka, Phys. Rev. B **49**, 4511 (1994); K. Kuriyama, R. Taguchi, K. Kushida, and K. Ushiyama, J. Cryst. Growth **198/199**, 802 (1999).
[7] K. Kuriyama, K. Nagasawa, and K. Kushida, J. Cryst. Growth **237/239**, 2019 (2002); K. Kuriyama, Y. Yamashita, T. Ishikawa, and K. Kushida, Phys. Rev. B **75**, 233204 (2007).
[8] K. Kushida, Y. Kaneko, and K. Kuriyama, Phys. Rev. B **70**, 233303 (2004); K. Kuriyama, Y. Kaneko, and K. Kushida, J. Cryst. Growth **275**, 395 (2005).
[9] K. Kuriyama, T. Ishikawa, and K. Kushida, *Proceedings of the 28th International Conference on Physics of Semiconductors*, AIP Conf. Proc. No. 1479 (AIP, New York, 2007).
[10] A. E. Carlsson, A. Zunger, and D. M. Wood, Phys. Rev. B **32**, 1386 (1985).
[11] D. M. Wood, A. Zunger, and R. de Grood, Phys. Rev. B **31**, 2570 (1985).
[12] S. H. Wei and A. Zunger, Phys. Rev. Lett. **56**, 528 (1986).
[13] M. C. Lan and P. Tao, Chin. Phys. Lett. **23**, 186 (2006).
[14] D. E. Ellis and G. S. Painter, Phys. Rev. B **2**, 2887 (1970).
[15] J. C. Slater, Phys. Rev. **81**, 385 (1951).
[16] J. C. Slater, *The Calculation of Molecular Orbitals* (Wiley, New York, 1979), Chap. 2.
[17] A. Rosen, D. E. Ellis, H. Adachi, and F. W. Averill, J. Chem. Phys. **65**, 3629 (1976).
[18] H. Adachi, M. Tsukada, and C. Satoko, J. Phys. Soc. Jpn. **45**, 875 (1978).
[19] C. Satoko, M. Tsukada, and H. Adachi, J. Phys. Soc. Jpn. **45**,

1333 (1978).
[20] H. Yoshida, R. Yoshimatsu, S. Watanabe, and K. Ogasawara, Jpn. J. Appl. Phys., Part 1 **45**, 146 (2006).
[21] Y. Liu, T. Fujiwara, H. Yukawa, and M. Morinaga, Solid State Ionics **126**, 209 (1999).
[22] S. Kawakami, M. Sasaki, H. Tabata, H. Shimooka, S. Kohiki, S. Matsushima, M. Oku, and T. Shishido, J. Alloys Compd. **359**, 278 (2003).
[23] The programs DVSCAT, BNDODR, NETC, and DOS used in this study are available from the CD-ROM attached to the book of Y. Kowada, I. Tanaka, H. Nakamatsu, and M. Mizuno, in *Hajimete-no-Denchijoutai Keisan*, edited by H. Adachi (Sankyo, Tokyo, 1999) (in Japanese).